ACS APPLIED BIO MATERIALS

www.acsabm.org Article

Ultrasound-Responsive Lipid Nanoplatform with Nitric Oxide and Carbon Monoxide Release for Cancer Sono-Gaso-Therapy

Yaw Opoku-Damoah, Zhi Ping Xu,* Hang T. Ta, and Run Zhang*

Cite This: *ACS Appl. Bio Mater.* 2024, 7, 7585−7594 Read Online

ACCESS | Metrics & More | Article Recommendations | Supporting Information

ABSTRACT: Local gas therapy is emerging as a potential cancer treatment approach due to its specificity as gas-containing molecules can be packed into a nanodelivery system to release the corresponding gaseous molecules around the tumor site upon a suitable stimulus. Single-gas therapy has been reported, while synergistic dual-gas therapy has rarely been reported. Herein, we report a dual-gas-containing nanoplatform for synergistic cancer gasotherapy upon ultrasound irradiation. First, a robust ultrasound-responsive lipid-coated nanosystem was prepared with suitable particle size and characteristics. A low-intensity ultrasound (1.25 W/cm^2) was found to simultaneously modulate carbon monoxide (CO) and nitric oxide (NO) release from the nanosystem in media and CT26 colon cancer cells for efficient therapeutic effect. The intracellular release promoted the overgeneration of reactive oxygen species (ROS) and triggered cancer cell apoptosis synergistically. The in vivo test demonstrated that the optimal dual-gas-containing formulation efficiently inhibited tumor growth (by ∼87%) at relatively low doses upon ultrasound irradiation (1.25 W/cm^2, 5 min). This therapeutic efficacy shows that the current responsive lipid-coated delivery system has potential for ultrasound-triggered dual-gas therapy of both superficially and deeply seated cancers.

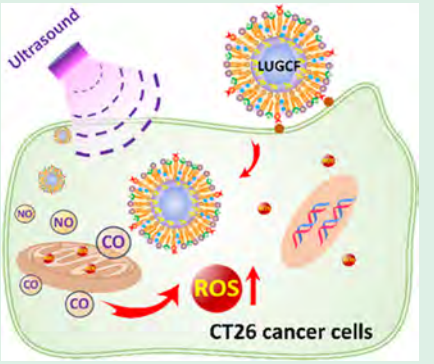

KEYWORDS: *gas therapy, low-intensity ultrasound, lipid delivery system, nitric oxide, carbon monoxide*

1. INTRODUCTION

Advanced techniques and strategies based on nanomaterial drug delivery for cancer therapy have continuously been evolved over the last few decades. Despite the innovation and progress so far, targeted drug delivery with low side effects is still a great challenge.[1−3] Noninvasive tumor targeting and controlled release with multifaceted nanoplatforms have proven to be promising in combating cancer.[3−5] Therapeutic agents that require specific responsive release patterns have been proven to be effective against cancer, but site-specific release in targeted tumor is still limited in various delivery systems.[3,6−9] In particular, therapeutic gases remain one of the most challenging agents for delivery because of the shapeless nature and difficulty in handling their release in biological tissues.[10−13] Fortunately, the advent of responsive gas-releasing molecules (GRMs) in recent years has paved the way for more efficient gas release systems that ensure safe administration, absorption, distribution, metabolism, and excretion of these gases for effective cancer gas therapy.[10,14−17]

Gas therapy has gained remarkable attention since many bioactive gas molecules have been detected in biological systems. These gas molecules, termed gasotransmitters, play various therapeutic and mediatory roles in living systems.[16,18,19] Therefore, they are identified and explored to increase their therapeutic potentials for conditions such as inflammation, cancer, and cardiovascular diseases.[20−24] These gasotransmitters include nitric oxide (NO), carbon monoxide (CO), hydrogen sulfide (H_2S), and sulfur dioxide (SO_2). NO is noted for its ability to downregulate the drug efflux-related P-glycoprotein and adenosine 5′-triphosphate-binding cassette transporters, which increases the accumulation and action of other drugs.[25,26] NO also contributes to combating drug resistance in multidrug-resistant (MDR) cancers via blood vessel stimulation around cancerous tissues and interfering with the dysregulated prosurvival/antiapoptotic NF-κB/Snail/YY1/RKIP/PTEN loop, which all contribute to help increase drug accumulation and effect.[27,28] CO possesses anticancer effects, which facilitate an anti-Warburg action by significantly elevating bioenergetics in cancer cells for metabolic exhaustion. Its action in the mitochondria facilitates reactive oxygen species (ROS) generation, resulting in mitochondrial destruction and eventual apoptosis.[29,30] CO also tightly binds to a variety of heme-containing proteins in the mitochondria, which is dependent on mitochondrial ROS signaling. The main challenge hinges on safe gas delivery without leakage in other biological tissues, which is now being well addressed by the advent of GRMs.[31] These GRMs are capable of holding gases

Received: August 16, 2024
Revised: October 28, 2024
Accepted: October 31, 2024
Published: November 7, 2024

before in situ cleavage in cancer cells.[32] Thus, a more target-specific approach is required for drug delivery by the use of responsive nanobased drugs.[33]

Responsive gas release with stimuli such as light and ultrasound is very promising because of the noninvasive nature of these techniques.[3,34,35] For example, near-infrared (NIR) light-responsive gas delivery systems have been developed in recent years for phototherapies, including photothermal and photodynamic therapies. Recently, ultrasound has been demonstrated in different therapeutic deliveries for triggering drug release at the tumor site;[35−39] ultrasound-responsive gas release delivery systems have not been explored yet. Nonetheless, ultrasound was used to release gases (CO or NO) attached to metal centers to produce nanophases such as metal sulfides, alloys, carbides, or metal oxides,[40−42] which is also dependent on the intensity of ultrasound.[43−45] More recently, it is demonstrated that CO is released from a CO release molecule (CORM) core encapsulated with a surfactant shell in the form of a micelle.[46] Similarly, NO is noted to release from *S*-nitrosothiol (GSNO) and similar SNO compounds in acidic conditions by ultrasound.[47] It has also been postulated that a little amount of CO is released from CORMs (such as CORM-3) in biological tissues with high levels of thiols such as cysteine, glutathione, and methionine via displacement of CO molecules by sulfur molecules.[48] This study suggests that thiols may stimulate the release of CO from the CORMs under ultrasound irradiation.

In this contribution, we elegantly investigated a lipid-coated delivery system that carries two therapeutic gas release molecules, including CORM and GSNO, for noninvasive ultrasound-responsive release of CO and NO simultaneously. In specific, we loaded hydrophilic GSNO on the surface of lanthanide-doped nanoparticles and coated them with 1,2-dioleoyl-*sn*-glycero-3-phosphate lipids (DOPA) to render amphiphilic for the loading of CORM ($C_{30}H_{49}N_3Mn(CO)_3Br$) in the lipid bilayer, as shown in Scheme 1. The lipid delivery system with folate targeting tumor cells has demonstrated its suitability for delivery and in situ responsive release of essential amounts of NO and CO molecules upon relatively low ultrasound irradiation (1.25 W/cm^2, 5 min). The nanoplatform was capable of triggering cancer apoptosis in both cellular and in vivo studies by pathways including ROS overgeneration from both gases. The ultrasound-triggered release of two therapeutic gases (CO and NO) in this work represents a new approach to cancer sono-gaso-therapy.

Scheme 1. Schematic Illustration of the Structure of the Lipid Nanoplatform and Ultrasound-Induced Intracellular Release of CO and NO from CORM and GSNO, Respectively, for Synergistic Cancer Sono-Gaso-Therapy

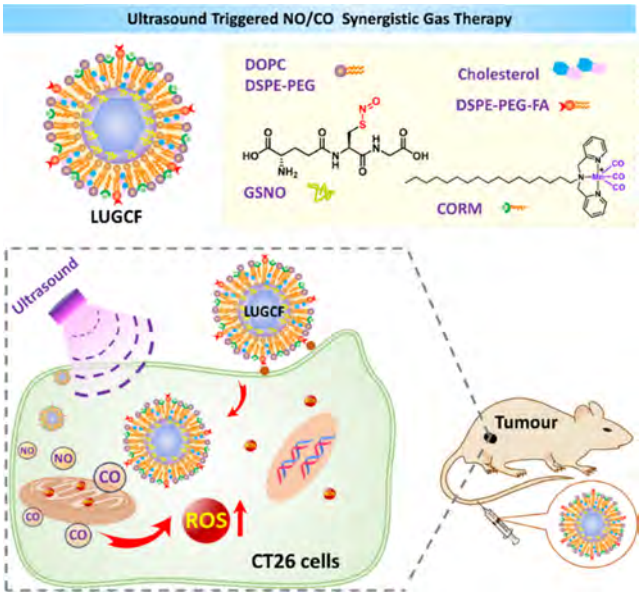

2. EXPERIMENTAL SECTION

2.1. Characterization of Lipid Nanoformulations. Lanthanide-doped UCNP nanoparticles (5 mg) were coated with GSNO (0.5−1.5 mg) and DOPA (0.4 mg) to form an amphiphilic intermediate (DOPA-UCNP@GSNO) according to previous methods.[49−51] The obtained nanoformulations, LUGCF (Lipid/UCNP/GSNO/CORM/FA), with varied mass ratios from 1:1 to 4:1 (GSNO:CORM) were dispersed in HEPES buffer for further applications. The morphology of the LUGCF-1:1 nanoformulation was visualized by a Hitachi HT7700A transmission electron microscope (TEM) via staining with 1% phosphotungsten acid (PTA) on copper grids. Fourier transform infrared (Thermo Scientific Nicolet 6700 FTIR) spectroscopy was employed to confirm the formation of nanomaterials and drug encapsulation. The surface ζ-potential and the particle size distribution were obtained by dynamic light scattering (DLS) (Nano-ZS Zetasizer, Malvern Instruments). The colloidal stability of LUGCF-1:1 nanoformulation in HEPES buffer was determined by measuring the particle size distribution for 12 days (2 day intervals). The concentration of the encapsulated CORM in nanoformulations was determined by inductively coupled plasma-optical emission spectroscopy (ICP-OES). GSNO was determined by elemental analysis of carbon, hydrogen, and nitrogen using a CHNS/O Elemental Analyzer (Thermo Scientific FLASH 2000 Analyzer).

2.2. Detection of Gas Release by Fluorescence Spectrophotometry. A ruthenium(II) complex-based NO-responsive luminescence probe (NOFP) was applied to determine NO release in situ.[52] Emission intensity of NOFP ($\lambda_{ex/em}$ = 450/600 nm) was recorded in a Shimadzu RF 5301-PC fluorescence spectrophotometer at various time points after ultrasound application at variable radiation intensities (1.25−5.0 W/cm^2) for 5 min. A CO-responsive fluorescence probe (COFP) was used to determine CO release from LUGCF.[53] COFP (10 μM) was added to the nanoformulation (15 μmol of CORM), and the fluorescence intensity ($\lambda_{ex/em}$ = 440/520 nm) was recorded after ultrasound application. The mixture in a quartz cuvette was sealed with parafilm throughout the experiment to prevent the escape of both gases post ultrasound application. A second ultrasound irradiation was applied after 2 h to determine the amount of CO and NO gases that were not released at the first ultrasound irradiation.

2.3. Intracellular Detection of Released Gases. Mice colorectal cancer CT26 cells (20,000/well) were seeded in 24-well plates and incubated at 37 °C for 24 h. Intracellular NO was determined by incubating the cells with cell culture media containing LUGCF-1:1 (45 μmol of GSNO). After incubation for 4 h, the respective media were discarded and fresh ones containing 10 μM of RuNO were added, which was followed by ultrasound application at 1.25 W/cm^2 for 5 min. Cells were continuously incubated for 2 h, washed, and collected in 150 μL of FACS buffer for flow cytometry analysis (Beckman Coulter FC 500) (λ_{ex} = 488 nm, λ_{em} = 575 nm). Cells without nanoformulation incubation and that with no ultrasound application were also assessed as controls. For qualitative observation, cells were incubated in 12-well plates with glass slides at the bottom, and the same incubation procedure was employed. Then, cells were fixed with 4% paraformaldehyde for fluorescence images (λ_{ex} = 460 nm, λ_{em} = 530 nm) in a fluorescent microscope (Olympus BX61 light microscope).

The same method was also employed for quantitative and qualitative CO detection in CT26 cells that were incubated with LUGCF-1:1 containing CORM (15 μmol), stained with 10 μM of

https://doi.org/10.1021/acsabm.4c01165
ACS Appl. Bio Mater. 2024, 7, 7585−7594

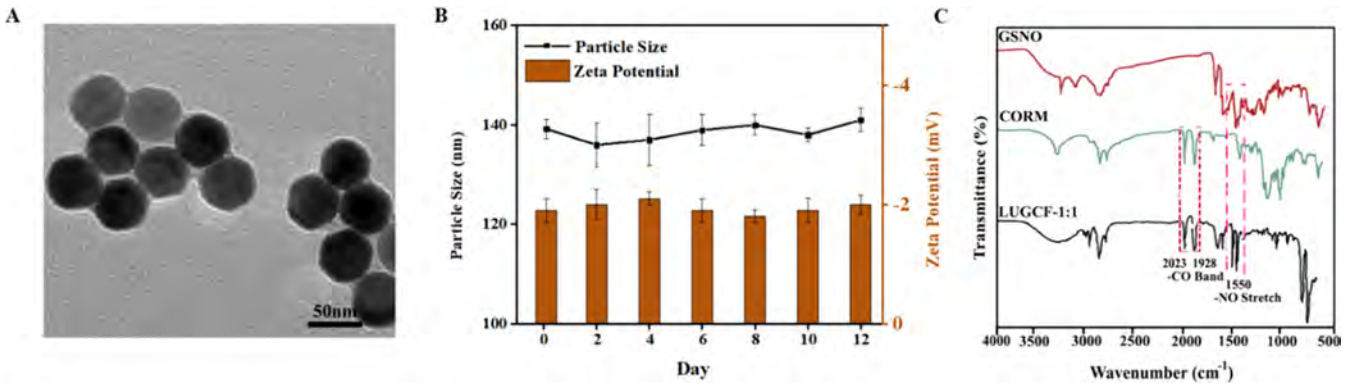

Figure 1. Particle characterization of nanoformulations (LUGCF-1:1). (A) TEM images of LUGCF nanoparticles; (B) nanoparticle colloidal stability with periodic size and surface ζ-potential measurements in 12 days; and (C) FTIR spectra of LUGCF-1:1 compared to GSNO and CORM.

COFP, and detected at λ_{em} = 525 nm. Cells were also observed microscopically to observe the morphological change upon ultrasound exposure.

2.4. Measurement of Cell Viability by MTT Assay. CT26 cells (1×10^4 cells/well) were seeded in 96-well plates with 100 μL of DMEM culture medium and incubated for 24 h. Then, media were replaced with FBS-free media containing various formulations (0−30 μg/mL of CORM/GSNO) and incubated for 4 h, followed by replacement of media with fresh ones. Then, cells were subjected to ultrasound irradiation and continuously incubated for 20 h (48 h in total). MTT assay was employed to determine the CT26 cell viability after treatment with LUGF, LUGF + US, LUCF, LUCF + US, LUGCF-1:1, and LUGCF-1:1 + US, where US represents ultrasound at 1.25 W/cm^2 for 5 min. After 48 h of incubation, 10 μL of MTT solution (5 mg/mL) was added to respective wells and incubated for another 4 h. Then, the medium in each well was replaced with 100 μL of DMSO to dissolve the formazan stain. The absorbance was measured at 570 nm using 670 nm as a fixed reference (Tecan Infinite M200 PRO Multimode Microplate Reader (Switzerland)). The cell viability was calculated accordingly.[54] The same MTT procedure was employed to compare the effectiveness of various formulations with the CORM:GSNO mass ratios of 1:1, 2:1, 3:1, and 4:1.

2.5. Intracellular ROS Detection. Quantitative ROS determination was performed by flow cytometry (Beckman Coulter FC 500) using the ROS probe (2′,7′-dichlorodihydrofluorescein diacetate -DCFH-DA, $\lambda_{ex/em}$ = 488/525 nm). CT26 cells at a density of 1×10^5 cell/well were incubated in 24-well plates for 24 h. Cell culture medium of each well was replaced with the fresh one containing LUGF, LUCF, or LUGCF-1:1 (CORM:GSNO 5/5 μg/mL), and the cells were then incubated for another 4 h. Then, media with nanoformulations were discarded and fresh media containing ROS probe (10 μM) were added in each well. Then, the ultrasound was applied for 5 min, followed by a second ultrasound application after 30 min of incubation post first ultrasound irradiation. Cells were collected and washed with PBS buffer three times and then redispersed in FACS buffer (150 μL) for flow cytometry analyses. The same procedure was adopted for ROS imaging, but cells were incubated in wells with glass slides on the bottom and fixed with 4% paraformaldehyde for 15 min after ultrasound treatment and staining before fluorescence imaging (λ_{em} = 525 nm).

2.6. Cell Apoptosis Assay in CT26 Cells. Cell apoptosis assay in CT26 cells was applied using an Annexin V-fluorescein isothiocyanate (FITC) assay kit (BD Biosciences Pharmingen) via flow cytometry. Typically, CT26 cells at a density of 1×10^5/well were seeded in 24-well plates for incubation at 37 °C for 24 h. Cells were then treated with media containing formulations (2.28/2.28 μg/mL of CORM/GSNO concentration) for 4 h. Cell culture media were then replaced with fresh media prior to ultrasound application (LUGF + US, LUCF + US, and LUGCF-1:1 + US). After a further 6 h incubation, a second ultrasound treatment was applied. The cells were continuously incubated for another 14 h and then harvested via centrifugation at 300g for 4 min. The cells were washed twice with PBS and resuspended in 100 μL of assay binding buffer. Annexin V-FITC and propidium iodide (PI) (5 μL each) were added to the cell suspension, and after 20 min of incubation in the dark, the contents were diluted with 400 μL of binding buffer. At least 10,000 cells were then analyzed in a flow cytometry per sample.

2.7. Evaluation of Therapeutic Effect In Vivo. All animal experiments in this work were performed following the procedures approved by the Animal Ethics Committee (AIBN/224/18) of The University of Queensland. Typically, 6−8 week old female BALB/c mice were housed with free access to water and food throughout the experiments. Tumor xenografts in BALB/c mice were obtained by subcutaneously injecting CT26 cells (2×10^6) in 100 μL of FBS-free cell culture medium on the right flank of mice. The tumor size and weight were monitored every other day, and its volume (V) was calculated by the formula $V = L \times W^2/2$, where L and W represent the longest and the shortest dimensions of the tumor, respectively, measured with a caliper.

After the tumor volume reached ∼100 mm^3, mice were randomly separated into six groups with n = 5 for each group, including groups of PBS, LUCGF-1:1, LUGF + US, LUCF + US, LUGCF-1:1 + US, and LUGCF-2:1 + US. The mice were then intravenously injected with nanoformulations containing 7.5 mg/kg of GSNO and/or 7.5 mg/kg of CORM in each dose at the tail vein. In comparison, LUGCF-2:1 + US with a dose of 10 mg/kg of GSNO and 5 mg/kg of CORM was also conducted. The nanoformulations were administered at days 0, 3, 6, and 9, and the ultrasound was applied at 1.25 W/cm^2 for 5 min at 12 and 24 h post injection. The therapeutic efficacy was assessed by monitoring the tumor volumes and body weights of all mice periodically. Major organs were excised for H&E staining to evaluate the safety of nanoformulations on day 12, and the tissues were visualized with an Olympio BX61 microscope.

For in vivo gas release and ROS assessment after tumors grew to ∼100 mm^3, CT26 tumor-bearing mice were intravenously injected with saline (100 μL) or LUGCF-1:1 (7.5 mg/kg GSNO and 7.5 mg/kg of CORM). Mice were intratumorally injected with 50 μL of the specific probe (2 mM) at 10 h post iv injection. Then, the ultrasound was applied at 12 h post iv injection of nanoformulation. After 30 min, mice were sacrificed accordingly, and tumors were harvested and imaged to record the fluorescence signals to determine in vivo CO release, NO release, and ROS generation.

2.8. Statistical Analysis. Data are presented as mean ± standard error of the mean (SEM) from at least triplicate experiments conducted in a parallel manner unless otherwise stated. The differences among various groups were analyzed using one-way analysis of variance (ANOVA), and the significance was indicated as *: $p < 0.05$, **: $p < 0.01$, and ***: $p < 0.001$.

https://doi.org/10.1021/acsabm.4c01165
ACS Appl. Bio Mater. 2024, 7, 7585−7594

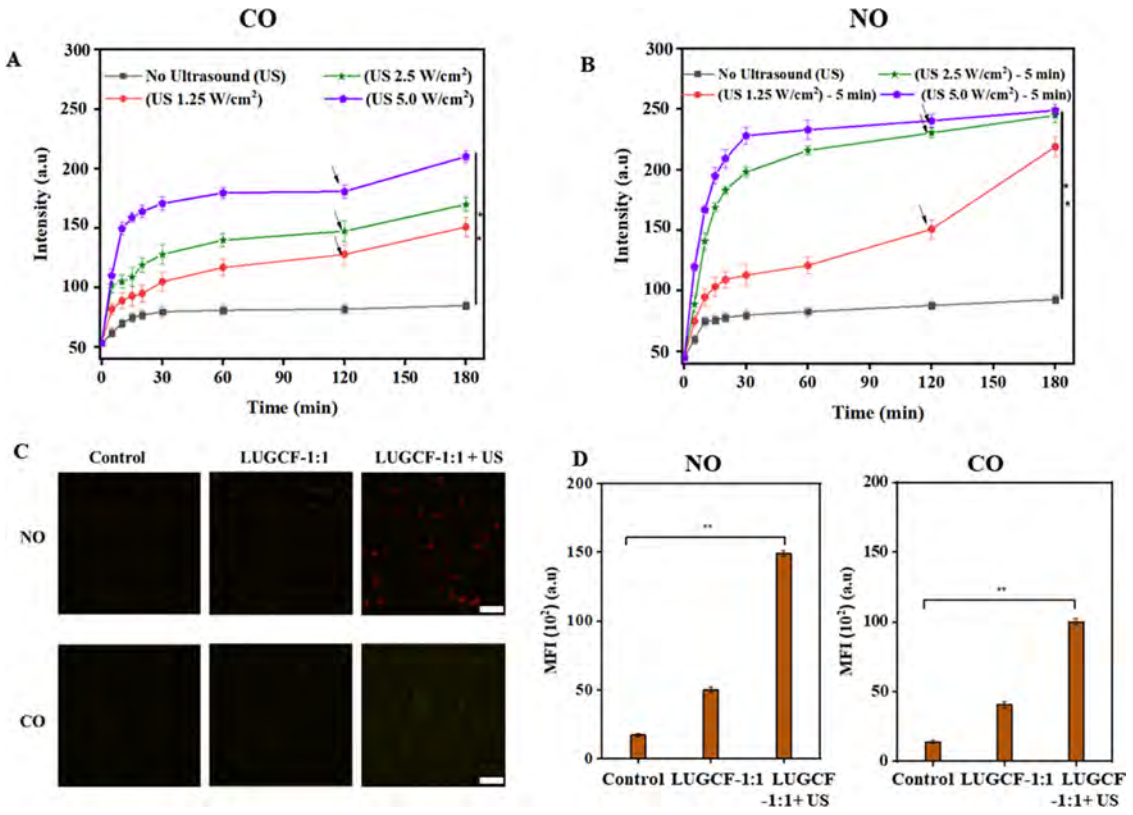

Figure 2. Ultrasound-responsive gas release from LUGCF-1:1 nanoformulation. (A) CO release profile of LUGCF-1:1 under different ultrasound conditions (detected by COFP at λ_{em} = 530 nm); arrows indicate the second application of ultrasound at 120 min. (B) NO release profile of LUGCF-1:1 with different ultrasound conditions (detected by NOFP at λ_{em} = 600 nm). (C) Fluorescent images at both blue and green excitation filters of LUGCF-1:1 and COPF/NOFP deposited CT26 cells with and without ultrasound application (1.25 W/cm^2 for 5 min); scale bar = 50 μm. (D) Flow cytometry data showing the quantitative determination of intracellular gases by probes. $^{**}p < 0.01$, $^{***}p < 0.001$ and $^{****}p < 0.0001$.

3. RESULTS AND DISCUSSION

3.1. Characteristics of Nanoformulations. Following the protocol developed in our recent research,[49] two therapeutic gas-releasing molecules GSNO (for NO) and CORM (for CO) were successfully incorporated into LUGCF that can target CT26 cancer cells for in situ ultrasound-mediated gas therapy (Scheme 1). Figure 1A shows the TEM image of LUGCF-1:1 (GSNO:CORM mass ratio of 1:1) with a thin lipid layer surrounding hexagonally shaped UCNPs. The particle size of all LUGCF samples with the GSNO/CORM mass ratio from 1:1 to 4:1 was within 131−137 nm, and the ζ-potential was slightly negative, which is in consistent with our previous research,[49] suggesting their suitability for in vivo cancer drug delivery. The particle size and ζ-potential of LUGCF-1:1 were kept quite constant during storage for 12 days at 4 °C in both buffer (Figure 1B) and cell culture medium (mimicking biological fluid) (Figure S1), indicating the excellent colloidal stability of the nanoformulations.

Both amphiphilic gas-releasing molecules (GSNO and CORM) were coloaded into lipid nanoparticles successfully, as confirmed by the FTIR spectra (Figure 1C). As seen in the spectra, the characteristic CO bands at 2023 and 1928 cm^{-1} were observed in both pure CORM and LUGCF-1:1 nanoformulation. Similarly, the NO band at 1550 cm^{-1} was also observed in GSNO and LUGCF-1:1. Furthermore, both drugs were quantified using elemental analysis. The mass percentages of loaded GSNO and CORM were 4.60 and 4.59 wt %, respectively, with the mass ratio being the same as that (1:1) in the initial CORM:GSNO formulation. A similar observation was found for LUGCF samples with the GSNO:CORM mass ratios of 2:1, 3:1, and 4:1. The loading of GSNO is probably achieved by being capped on oleic acid-free UCNPs through coordination and electronic attractions of GSNO's terminal carboxylates to lanthanide ions,[55] and the terminal-HPO_4^- group of DOPA allows the electrostatic interaction with the UCNP's surface.[56]

3.2. Ultrasound-Responsive Gas Release. The gas release profiles of LUGCF-1:1 were determined by observing the increased fluorescence of COFP and NOFP. As seen in Figure 2A, there was a minimal change in the COFP probe's fluorescence within 30 min in the absence of ultrasound stimuli. Upon an ultrasound application at 1.25 W/cm^2 for 5 min, there was a quick increase in COFP's fluorescence intensity of COFP in a 30 min incubation, which slowly increased in 30−120 min. Upon the second ultrasound application, the fluorescence intensity increased to some degree. Similarly, increasing the ultrasound intensity (from 1.25 to 2.5 and 5.0 W/cm^2) resulted in more CO release (Figure 2A). The second ultrasound application at 5.0 W/cm^2 further released some CO, suggesting that not all of the gas molecules were activated to release CO even upon two ultrasound irradiations.

NO release was quite similar but appeared more efficient. In particular, the second ultrasound application at 2.5 or 5 W/cm^2 did not increase the fluorescence conspicuously (Figure 2B), suggesting that almost all NO molecules were released at the power of >2.5 W/cm^2. In contrast, the second application at 1.25 W/cm^2 significantly increased the NO release. Overall,

https://doi.org/10.1021/acsabm.4c01165
ACS Appl. Bio Mater. 2024, 7, 7585−7594

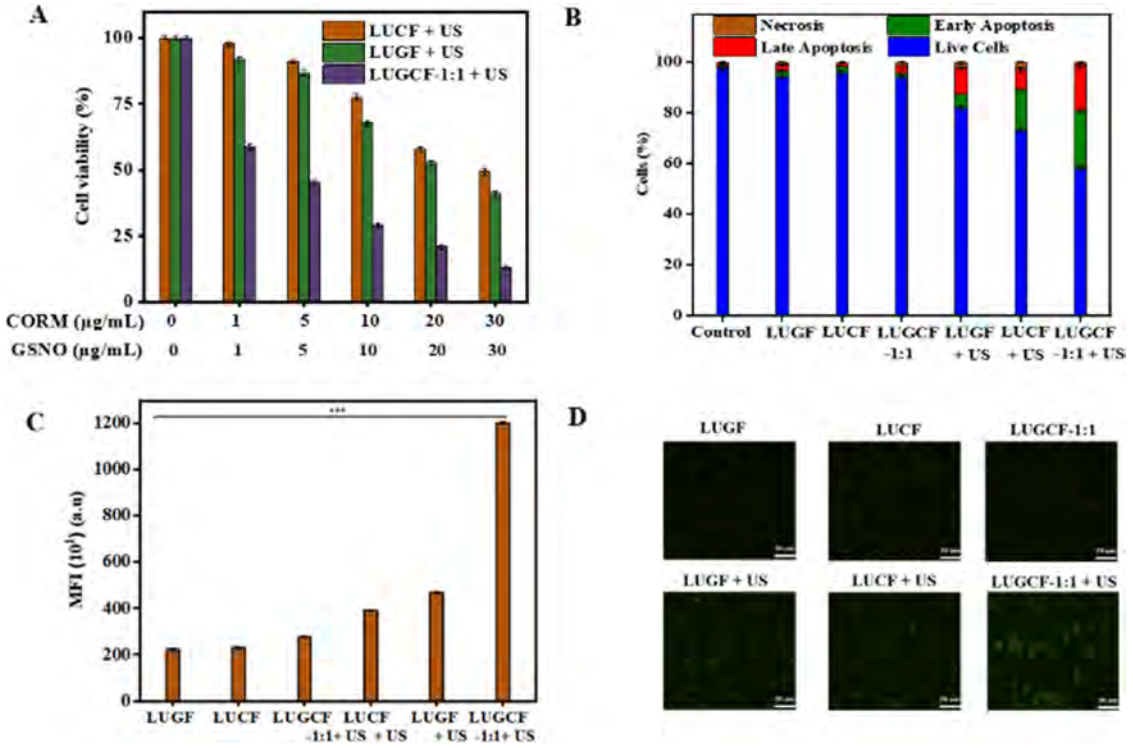

Figure 3. Cytotoxicity studies in CT26 cells. (A) Cell apoptosis assay of various GSNO/CORM lipid nanoformulations after 24 h of incubation. (B) CT26 cell apoptosis assay for various nanoformulations after 24 h of total incubation. (C) Flow cytometry analysis of intracellular ROS after nanoformulation incubation and DCFH-DA staining. (D) Fluorescence images of CT26 cells treated with various nanoformulations and DCFH-DA. Nanoparticles replaced with fresh media after 4 h and ultrasound groups (+US) treated twice at 4 and 6 h for 5 min (1.25 W/cm^2). Scale bar = 50 μm.

the NO release is slightly more efficient than the CO release upon the same ultrasound stimulation.

Figure 2C shows a similar release pattern for LUGCF-1:1 within cells upon ultrasound irradiation. There was a very low intracellular fluorescence of both gas probes in the control group and the LUGCF-1:1 group. In contrast, upon ultrasound application to the cells treated with LUGCF-1:1 for 4 h, clear fluorescent cells were observed, showing that both gases were released in cells. Relatively, the intracellular NOFP fluorescence is stronger than that of COFP. This has been further confirmed by flow cytometry data of two intracellular fluorescence signals. The cellular MFI of both probes upon treatment with LUGCF-1:1 + US was significantly higher than that treated with LUGCF-1:1 (Figure 2D). For cellular detection (CT26 cells), a less invasive power (1.25 W/cm^2 for 5 min) was selected to avoid damage to the cells, while this power is strong enough to release both gas molecules in substantial amounts (Figure 2A,B).

3.3. In Vitro Cancer Therapy. Of different types of therapeutic gases, CO has been known to accelerate cellular respiration and promote the massive consumption of O_2 and ATP to trigger the production and accumulation of mitochondrial ROS for tumor cell apoptosis. NO is one of the key reactive nitrogen species (RNS) that can rapidly react with ROS (e.g., superoxide) to produce highly reactive species (e.g., peroxynitrite), resulting in further damage to cancer cells through nitrosation of mitochondria and DNA, inhibiting cellular respiration. To exploit their therapeutic effects, ultrasound-triggered gas therapy was assessed to confirm the individual and synergistic effects of NO and CO gases on CT26 cells. Note that single drug formulations (LUCF and LUGF) and combination formulation (LUGCF-1:1) at 20−30 μg/mL for each prodrug did not obviously affect the cell viability without ultrasound application (Figure S2B), indicating the relative safety of the nanoformulations. Applying the ultrasound for the sample total energy on cells treated with LUCF (CORM) for 4 h at 1.25 or 2.5 W/cm^2 resulted in 85−90 and 75−80% cell viabilities, respectively, demonstrating that the released CO induced cell apoptosis to some degree. In contrast, for cells treated with LUGF (NO carrier), two ultrasound applications at 1.25 W/cm^2 for 5 min led to a slightly lower cell viability than ultrasound applications twice at 2.5 W/cm^2 for 2.5 min and once at 2.5 W/cm^2 for 5 min (Figure S2B), due to the release of more NO at the lower power for a long time (Figure 2B).

Figure 3A shows that the cell viability is dependent on the doses of CORM and GSNO with the ultrasound application (twice at 1.25 W/cm^2 for 5 min). The higher the dose of the single-gas carrier, the lower the cell viability (Table S1), with the IC_{50} values being 27.7 μg/mL for LUC + US and 22.4 μg/mL for LUGF + US (Table S2). When CORM and GSNO were coloaded at the mass ratio of 1:1 (LUGCF-1:1 + US), the same doses caused much lower cell viability (Figure 3A), with the IC_{50} value being reduced to 2.28 μg/mL for both gas prodrugs (Table S2). Significantly, two gas prodrugs seemed to have strong synergy at all doses in the combined nanoformulation as the combination index was 1.41−1.95 (Table S3) as of the contributions from both NO and CO. Specifically, the released CO could induce excessive ROS production and accumulation in mitochondria through accelerating cellular respiration to consume O_2 and ATP, while the released NO reacts with ROS to produce highly

https://doi.org/10.1021/acsabm.4c01165
ACS Appl. Bio Mater. 2024, 7, 7585−7594

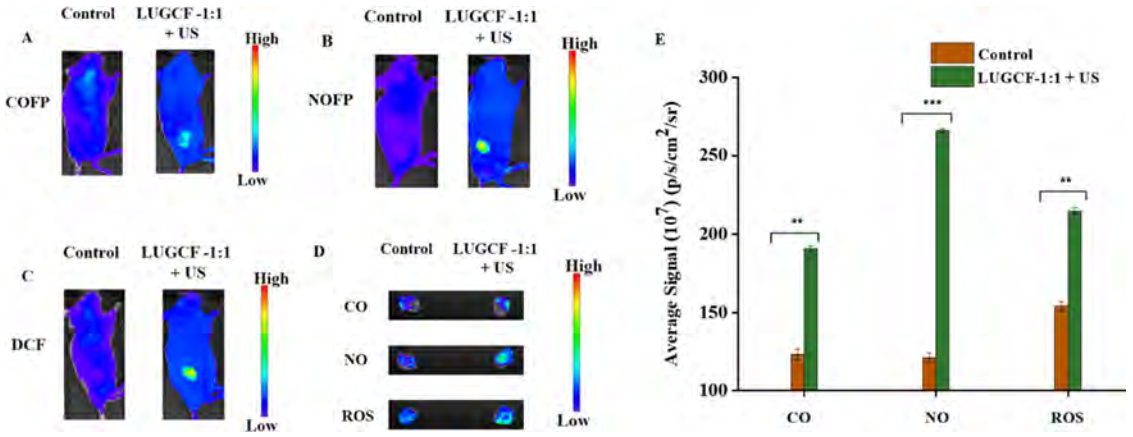

Figure 4. Mechanism of NO and CO release upon ultrasound application. (A) Detection of CO gas release by COFP fluorescence in vivo after 12 h of administration of nanoformulation and ultrasound irradiation. (B) Detection of NO gas release by NOFP fluorescence in vivo after the administration of nanoformulation and ultrasound irradiation. (C) In vivo and ex vivo detection of ROS by DCFH-DA fluorescence after the administration of nanoformulation and ultrasound irradiation. (D) Ex vivo fluorescent images of excised tumors from mice after in vivo monitoring of CO and NO release as well as ROS detection. (E) Fluorescence radiance intensity of signals in tumors after animals were sacrificed. Ultrasound power was 1.25 W/cm^2 for 5 min.

reactive nitrogen species for nitrosation of mitochondria and DNA to further inhibit cancer cell growth.

Furthermore, the CO and NO synergistic effects on CT26 cell death were also found for LUGCF samples at the GSNO:CORM mass ratios of 2:1, 3:1, and 4:1. As shown in Figure S3, the viability of cells treated upon LUGCF-1:1 + US and LUGCF-2:1 + US was comparable but much lower than that upon treatment with LUGCF-3:1 + US and LUGCF-4:1 + US at 10 and 20 μg/mL of the total [GSNO + CORM] dose, respectively. Significantly, in comparison with the LUCG and LUGF (Figure S4), the two prodrugs had a strong synergistic effect in the LUGCF-1:1 + US and LUGCF-2:1 + US treatments, as reflected by the high combination index (1.60−1.95 and 1.54−1.63) (Table S1). However, there seemed to be only an additive effect between the two prodrugs in the LUGCF-3:1 + US and LUGCF-4:1 + US treatments as the combination index was 0.95−1.22 (Table S1). Taking the combination index into consideration, LUGCF-1:1 was selected in the work for further therapeutic effect investigations.

The cell death induction was confirmed by apoptotic assessments via quantifying the percentage of necrotic, early, and late apoptosis cells. As shown in Figures 3B and S5, the LUGCF-1:1 + US treatment at its calculated IC_{50} concentration led to high percentages of late and early apoptotic cells. Similarly, LUGF + US and LUCF + US treatments also produced some late and early apoptotic cells. Note that there were less necrotic cells in all cases, demonstrating the relatively noninvasive damage of the combination treatment. Consistently, the intracellular ROS generation (Figure 3C) upon the LUGCF-1:1 + US treatment was the highest, about 3-fold higher than that of LUGF + US and LUCF + US. As shown in Figure 3D, a very prominent intracellular fluorescence was observed for the LUGCF-1:1 + US group, while less visible fluorescent cells were found upon treatments with single-gas prodrug-loaded formulations (LUCF and LUGF). This suggests that NO and CO together induce ROS generation more efficiently, which is pivotal in driving the therapeutic action of nanoformulation.

3.4. In Vivo Cancer Therapy. CO and NO gases from the LUGCF-1:1 nanoformulation upon ultrasound application were further assessed in a tumor-bearing mouse model. Figure 4A shows that there were some released CO molecules from the CORM as compared to the control group upon US treatment at 12 h post intravenous injection. NO release in mouse tumors was much higher compared to that in the control group (Figure 4B). Furthermore, the ROS in the tumor tissue was very clearly observed via its fluorescent probe upon the LUGCF-1:1 + US treatment (Figure 4C). Similar phenomena were observed in the ex vivo tumor images of both CO and NO probes (Figure 4D,E), showing significant NO and CO released upon US irradiation in the LUGCF-1:1 + US group. These consistent data demonstrate that the released CO/NO gases promote ROS generation and further induce cell death.

Figure 5A summarizes the tumor volume changes of six groups of mice during the treatment. Clearly, the injection of the LUGCF-1:1 formulation did not inhibit tumor growth compared to the control group, indicating that the formulation had a negligible antitumor effect. Upon the ultrasound application, treatments with single-gas prodrug formulation (LUCF + US and LUGF + US) for 4 times (30 mg/kg of CORM or GSNO in total) produced some antitumor effect, with the tumor volume reduced by 43 and 48%, respectively, at day 12. The lower therapeutic action upon the LUCF + US treatment is probably because the ultrasound-triggered release of CO is slightly limited as compared to NO release from the LUGF + US treatment (Figure 2A,B).

The combination of CO and NO gas prodrugs significantly enhanced the therapeutic efficiency to about 87% and 80% tumor inhibition upon treatments of LUGCF-1:1 + US and LUGCF-2:1 + US, respectively, at the same total doses of each prodrug. The LUGCF-1:1 + US treatment seems superior to LUGCF-2:1 + US, consistent with the slightly higher cytotoxicity (Figure S2A) and higher synergistic effect between the two therapeutic gases (Table S3) in LUGCF-1:1 formulation. It seems that the relatively higher amount of CORM (30 vs 20 mg/kg) not only offsets the reduced effect due to the lower GSNO amount (30 vs 40 mg/kg) but also provides more potent CO gas molecules for synergistic tumor therapy. The same trend was observed for the change of the weight of tumor tissues collected at day 12 (Figure 5B). A

https://doi.org/10.1021/acsabm.4c01165
ACS Appl. Bio Mater. 2024, 7, 7585−7594

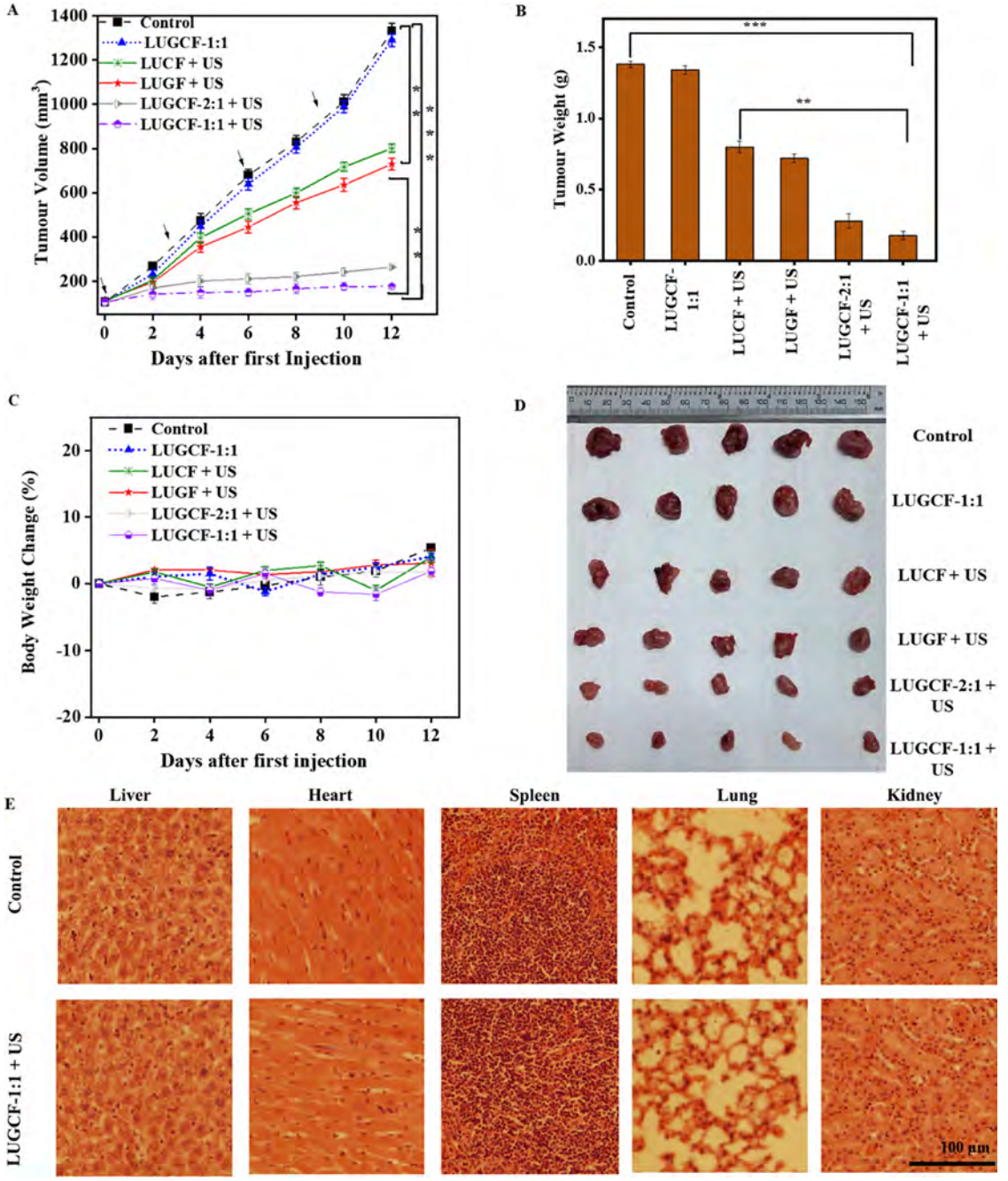

Figure 5. In vivo therapeutic effect. (A) Tumor volume throughout the study. Arrows indicate the day of drug administration (day 3, day 6, day 9). (B) Tumor weights of mice after the treatment. (C) Percentage body weight changes within 12 days of treatment. (D) Images of tumors harvested at 12 days after drug and saline injection; iv injection at days 0, 3, 6, and 9 at 10/7.5 mg/kg of GSNO and 5/7.5 mg/kg of CORMs, and ultrasound at 12 and 24 h after injection (1.25 W/cm^2 for 5 min) for groups with ultrasound irradiation. (E) Histopathological images of various mice organs obtained after drug treatment. Scale bar = 100 μm *: $p < 0.05$, **: $p < 0.01$, and ***: $p < 0.001$.

significant difference was noted by comparing LUGCF-1:1 + US and LUGCF-2:1 + US groups (0.2−0.3 g) with single drug groups (LUCF + US and LUGF + US) (0.7−0.8 g) and the LUGCF-1:1 group (1.3 g). The tumor weight in the LUGCF-1:1 + US treatment group is approximately 14.5% of that in the control group, indicating a significant inhibition of tumor growth with the sono-gaso-therapy.

During the in vivo experiment, there were no significant body weight variations with respect to tumor growth (Figure 5C), confirming that the injected LUGCF-1:1 and LUGCF-2:1 nanoformulations containing both therapeutic gas prodrugs did not affect the integrity of various organ tissues, indicating that the UCNP-based nanoformulations are biocompatible. Furthermore, the sizes of tumors as observed visually were consistent with the tumor volume and tumor weight results (Figure 5D). Herein, the size of tumors for the groups treated with LUGCF-1:1 + US was significantly smaller than the LUGF + US, LUCF + US, and the LUGCCG-2:1 groups, even though the latter groups mentioned had some observable tumor reduction effect as compared to the control group that received only saline. Overall, it was observed that the LUGCF-1:1 + US group had the smallest sizes of tumors as observed

https://doi.org/10.1021/acsabm.4c01165
ACS Appl. Bio Mater. 2024, 7, 7585−7594

visually. The microscopic images of various H&E-stained tissues as shown in Figure 5E suggest that there was no significant systemic toxicity of any of the materials administered as the effect of the final nanoparticle LUGCF-1:1 + US on various organs' pathophysiology was similar to that of the control group that received saline under the same conditions. This suggests that this nanoformulation is biocompatible within the period of administration.

4. CONCLUSIONS

In this research, an ultrasound-responsive lipid nanoplatform for codelivery of two gas-releasing molecules was developed with folate targeting CT26 cancer cells. The research has demonstrated that nanoformulation LUGCF-1:1 synergistically enhanced the dual therapeutic effect as compared to other mass ratios (2:1, 3:1, and 4:1) when ultrasound was applied. Both gases were released responsively upon ultrasound application, and the optimal ultrasound power (1.25 W/cm^2) was identified in terms of gas release and damage to the cells. The released gases produced a characteristic therapeutic effect on CT26 cells both in vitro and in vivo, probably via promoting overgeneration ROS. The two prodrugs produced a strong synergistic effect on cancer cell apoptosis upon ultrasound applications. This synergistic effect enabled the LUGCF-1:1 + US treatment to efficiently inhibit tumor growth in the mouse model even at relatively low doses upon mild-power ultrasound irradiation. In summary, we produced the first ultrasound-responsive codelivery system to codeliver CO and NO prodrugs for enhanced cancer sono-gaso-therapy.

■ ASSOCIATED CONTENT

Supporting Information

The Supporting Information is available free of charge at https://pubs.acs.org/doi/10.1021/acsabm.4c01165.

Materials and performance characterizations, including colloidal stability, cell viability, MTT assay, flow cytometry analysis, tables of the MTT data summary, IC_{50}, combination therapy analysis, and further details of the experiments (PDF)

■ AUTHOR INFORMATION

Corresponding Authors

Zhi Ping Xu − *Australian Institute for Bioengineering and Nanotechnology, The University of Queensland, Brisbane, QLD 4072, Australia; Institute of Biomedical Health Technology and Engineering and Institute of Systems and Physical Biology, Shenzhen Bay Laboratory, Shenzhen 518107, P. R. China;* orcid.org/0000-0001-6070-5035; Email: gordonxu@uq.edu.au

Run Zhang − *Australian Institute for Bioengineering and Nanotechnology, The University of Queensland, Brisbane, QLD 4072, Australia;* orcid.org/0000-0002-0943-824X; Email: r.zhang@uq.edu.au

Authors

Yaw Opoku-Damoah − *Australian Institute for Bioengineering and Nanotechnology, The University of Queensland, Brisbane, QLD 4072, Australia*

Hang T. Ta − *Australian Institute for Bioengineering and Nanotechnology, The University of Queensland, Brisbane, QLD 4072, Australia; School of Environment and Science, Griffith University, Brisbane, QLD 4111, Australia;* orcid.org/0000-0003-1188-0472

Complete contact information is available at: https://pubs.acs.org/10.1021/acsabm.4c01165

Author Contributions

The manuscript was written through contributions of all authors. All authors have given approval to the final version of the manuscript.

Funding

This work was supported by the National Health and Medical Research Council (APP1175808) and the Australian Research Council (ARC) Discovery Projects (DP190103486).

Notes

The authors declare no competing financial interest.

■ ACKNOWLEDGMENTS

Y.O.-D. gratefully acknowledges the Australian Government Research Training Program Scholarship (RTP). The authors also extend their thanks to the facilities and the technical assistance of the Australian Microscopy and Microanalysis Research Facility at the Centre for Microscopy and Microanalysis (CMM), the Australian National Fabrication Facility (QLD Node), and the Centre of Advance Imaging, The University of Queensland.

■ REFERENCES

(1) Hartshorn, C. M.; Bradbury, M. S.; Lanza, G. M.; Nel, A. E.; Rao, J.; Wang, A. Z.; Wiesner, U. B.; Yang, L.; Grodzinski, P. Nanotechnology Strategies To Advance Outcomes in Clinical Cancer Care. *ACS Nano* **2018**, *12* (1), 24−43.

(2) Rosenblum, D.; Joshi, N.; Tao, W.; Karp, J. M.; Peer, D. Progress and challenges towards targeted delivery of cancer therapeutics. *Nat. Commun.* **2018**, *9* (1), No. 1410.

(3) Zhao, W.; Zhao, Y.; Wang, Q.; Liu, T.; Sun, J.; Zhang, R. Remote Light-Responsive Nanocarriers for Controlled Drug Delivery: Advances and Perspectives. *Small* **2019**, *15* (45), No. 1903060.

(4) Wang, R.; Zhang, C.; Li, J.; Huang, J.; Opoku-Damoah, Y.; Sun, B.; Zhou, J.; Di, L.; Ding, Y. Laser-triggered polymeric lipoproteins for precision tumor penetrating theranostics. *Biomaterials* **2019**, *221*, No. 119413.

(5) Liu, J.; Zhang, R.; Xu, Z. P. Nanoparticle-Based Nanomedicines to Promote Cancer Immunotherapy: Recent Advances and Future Directions. *Small* **2019**, *15* (32), No. 1900262.

(6) Tang, Q.; Yu, B.; Gao, L.; Cong, H.; Song, N.; Lu, C. Stimuli Responsive Nanoparticles for Controlled Anti-cancer Drug Release. *Curr. Med. Chem.* **2018**, *25* (16), 1837−1866.

(7) Poelma, S. O.; Oh, S. S.; Helmy, S.; Knight, A. S.; Burnett, G. L.; Soh, H. T.; Hawker, C. J.; de Alaniz, J. R. Controlled drug release to cancer cells from modular one-photon visible light-responsive micellar system. *Chem. Commun.* **2016**, *52* (69), 10525−10528.

(8) Wang, X.; Zhang, J.; Zheng, K.; Du, Q.; Wang, G.; Huang, J.; Zhou, Y.; Li, Y.; Jin, H.; He, J. Discovering metabolic vulnerability using spatially resolved metabolomics for antitumor small molecule-drug conjugates development as a precise cancer therapy strategy. *J. Pharm. Anal.* **2023**, *13* (7), 776−787.

(9) Chen, B.; Zhao, Y.; Lin, Z.; Liang, J.; Fan, J.; Huang, Y.; He, L.; Liu, B. Apatinib and gamabufotalin co-loaded lipid/Prussian blue nanoparticles for synergistic therapy to gastric cancer with metastasis. *J. Pharm. Anal.* **2024**, *14* (5), No. 100904.

(10) Chung, M. F.; Chia, W. T.; Wan, W. L.; Lin, Y. J.; Sung, H. W. Controlled Release of an Anti-inflammatory Drug Using an Ultrasensitive ROS-Responsive Gas-Generating Carrier for Localized

Inflammation Inhibition. *J. Am. Chem. Soc.* **2015**, *137* (39), 12462−12465.
(11) Wu, D.; Wan, M. A novel ultrasonic-triggered drug release and tracked drug delivery system based on gas-filled BSA microbubbles and gelatin nanogels. *J. Controlled Release* **2015**, *213*, No. e24.
(12) Haznar-Garbacz, D.; Garbacz, G.; Eisenacher, F.; Klein, S.; Weitschies, W. A novel liquefied gas based oral controlled release drug delivery system for liquid drug formulations. *Eur. J. Pharm. Biopharm.* **2012**, *81* (2), 334−338.
(13) He, Q. Precision gas therapy using intelligent nanomedicine. *Biomater. Sci.* **2017**, *5* (11), 2226−2230.
(14) Chung, M. F.; Chia, W. T.; Liu, H. Y.; Hsiao, C. W.; Hsiao, H. C.; Yang, C. M.; Sung, H. W. Inflammation-induced drug release by using a pH-responsive gas-generating hollow-microsphere system for the treatment of osteomyelitis. *Adv. Healthcare Mater.* **2014**, *3* (11), 1854−1861.
(15) Zhang, Z.; Zhang, L.; Huang, C.; Guo, Q.; Zuo, Y.; Wang, N.; Jin, X.; Zhang, L.; Zhu, D. Gas-generating mesoporous silica nanoparticles with rapid localized drug release for enhanced chemophotothermal tumor therapy. *Biomater. Sci.* **2020**, *8* (23), 6754−6763.
(16) Yao, X.; Yang, B.; Xu, J.; He, Q.; Yang, W. Novel gas-based nanomedicines for cancer therapy. *View* **2022**, *3* (1), No. 20200185.
(17) Fraix, A.; Sortino, S. Photoactivable Platforms for Nitric Oxide Delivery with Fluorescence Imaging. *Chem. - Asian J.* **2015**, *10* (5), 1116−1125.
(18) Alimoradi, H.; Greish, K.; Gamble, A. B.; Giles, G. I. Controlled Delivery of Nitric Oxide for Cancer Therapy. *Pharm. Nanotechnol.* **2019**, *7* (4), 279−303.
(19) López-Sánchez, L. M.; Mena, R.; Guil-Luna, S.; Mantrana, A.; Penarando, J.; Toledano-Fonseca, M.; Conde, F.; De la Haba-Rodriguez, J. R.; Aranda, E.; Rodriguez-Ariza, A. Nitric oxide-targeted therapy inhibits stemness and increases the efficacy of tamoxifen in estrogen receptor-positive breast cancer cells. *Lab. Invest.* **2021**, *101* (3), 292−303.
(20) Fu, J.; Wu, Q.; Dang, Y.; Lei, X.; Feng, G.; Chen, M.; Yu, X. Y. Synergistic Therapy Using Doxorubicin-Loading and Nitric Oxide-Generating Hollow Prussian Blue Nanoparticles with Photoacoustic Imaging Potential Against Breast Cancer. *Int. J. Nanomed.* **2021**, *16*, 6003−6016.
(21) Tozer, G. M.; Everett, S. A. Nitric oxide in tumour biology and cancer therapy. Part 1: Physiological aspects. *Clin. Oncol.* **1997**, *9* (5), 282−293.
(22) Ren, H.; Yang, Q.; Yong, J.; Fang, X.; Yang, Z.; Liu, Z.; Jiang, X.; Miao, W.; Li, X. Mitochondria targeted nanoparticles to generate oxygen and responsive-release of carbon monoxide for enhanced photogas therapy of cancer. *Biomater. Sci.* **2021**, *9* (7), 2709−2720.
(23) Sakla, R.; Jose, D. A. Vesicles Functionalized with a CO-Releasing Molecule for Light-Induced CO Delivery. *ACS Appl. Mater. Interfaces* **2018**, *10* (16), 14214−14220.
(24) Tabish, T. A.; Hussain, M. Z.; Zervou, S.; Myers, W. K.; Tu, W.; Xu, J.; Beer, I.; Huang, W. E.; Chandrawati, R.; Crabtree, M. J.; Winyard, P. G.; Lygate, C. A. S-nitrosocysteamine-functionalised porous graphene oxide nanosheets as nitric oxide delivery vehicles for cardiovascular applications. *Redox Biol.* **2024**, *72*, No. 103144.
(25) Wang, H.; Wang, L.; Xie, Z.; Zhou, S.; Li, Y.; Zhou, Y.; Sun, M. Nitric Oxide (NO) and NO Synthases (NOS)-Based Targeted Therapy for Colon Cancer. *Cancers* **2020**, *12* (7), 1881.
(26) Rapozzi, V.; Della Pietra, E.; Zorzet, S.; Zacchigna, M.; Bonavida, B.; Xodo, L. E. Nitric oxide-mediated activity in anti-cancer photodynamic therapy. *Nitric Oxide* **2013**, *30*, 26−35.
(27) Li, S.; Song, X.; Zhu, W.; Chen, Y.; Zhu, R.; Wang, L.; Chen, X.; Song, J.; Yang, H. Light-Switchable Yolk−Mesoporous Shell UCNPs@MgSiO3 for Nitric Oxide-Evoked Multidrug Resistance Reversal in Cancer Therapy. *ACS Appl. Mater. Interfaces* **2020**, *12* (27), 30066−30076.
(28) Du, Z.; Mao, Y.; Zhang, P.; Hu, J.; Fu, J.; You, Q.; Yin, J. TPGS−Galactose-Modified Polydopamine Co-delivery Nanoparticles of Nitric Oxide Donor and Doxorubicin for Targeted Chemo−Photothermal Therapy against Drug-Resistant Hepatocellular Carcinoma. *ACS Appl. Mater. Interfaces* **2021**, *13* (30), 35518−35532.
(29) Zhou, Y.; Zhang, W.; Wang, X.; Li, P.; Tang, B. Recent Progress in Small-Molecule Fluorescence and Photoacoustic Dual-Modal Probes for the In-Vivo Detection of Bioactive Molecules. *Chem. - Asian J.* **2022**, *17* (10), No. e202200155.
(30) Alanazi, M.; Yong, J.; Wu, M.; Zhang, Z.; Tian, D.; Zhang, R. Recent Advances in Detection of Hydroxyl Radical by Responsive Fluorescence Nanoprobes. *Chem. - Asian J.* **2024**, *19* (8), No. e202400105.
(31) Liu, C.; Du, Z.; Ma, M.; Sun, Y.; Ren, J.; Qu, X. Carbon Monoxide Controllable Targeted Gas Therapy for Synergistic Anti-inflammation. *iScience* **2020**, *23* (9), No. 101483.
(32) Jin, D.; Zhang, J.; Huang, Y.; Qin, X.; Zhuang, J.; Yin, W.; Chen, S.; Wang, Y.; Hua, P.; Yao, Y. Recent advances in the development of metal-organic framework-based gas-releasing nano-platforms for synergistic cancer therapy. *Dalton Trans.* **2021**, *50* (4), 1189−1196.
(33) Opoku-Damoah, Y.; Assanhou, A. G.; Sooro, M. A.; Baduweh, C. A.; Sun, C.; Ding, Y. Functional Diagnostic and Therapeutic Nanoconstructs for Efficient Probing of Circulating Tumor Cells. *ACS Appl. Mater. Interfaces* **2018**, *10* (17), 14231−14247.
(34) Xie, A.; Hanif, S.; Ouyang, J.; Tang, Z.; Kong, N.; Kim, N. Y.; Qi, B.; Patel, D.; Shi, B.; Tao, W. Stimuli-responsive prodrug-based cancer nanomedicine. *EBioMedicine* **2020**, *56*, No. 102821.
(35) Wu, M.; Yong, J.; Zhang, H.; Wang, Z.; Xu, Z. P.; Zhang, R. 2D Ultrathin Iron Doped Bismuth Oxychloride Nanosheets with Rich Oxygen Vacancies for Enhanced Sonodynamic Therapy. *Adv. Healthcare Mater.* **2023**, *12* (30), No. 2301497.
(36) Schroeder, A.; Kost, J.; Barenholz, Y. Ultrasound, liposomes, and drug delivery: principles for using ultrasound to control the release of drugs from liposomes. *Chem. Phys. Lipids* **2009**, *162* (1−2), 1−16.
(37) Bohara, S.; Rohner, N.; Budziszewski, E.; Suthakorn, J.; von Recum, H. A.; Exner, A. A. Ultrasound Triggered Drug Release from Affinity-Based beta-Cyclodextrin Polymers for Infection Control. *Ann. Biomed Eng.* **2021**, *49* (9), 2513−2521.
(38) Sun, Q.; Song, W.; Gao, Y.; Ding, R.; Shi, S.; Han, S.; Li, G.; Pei, D.; Li, A.; He, G. A telluroviologen-anchored tetraphenylporphyrin as sonosensitizer for periodontitis sonodynamic therapy. *Biomaterials* **2024**, *304*, No. 122407.
(39) Wang, Z.; Wang, X.; Chang, M.; Guo, J.; Chen, Y. Ultrasound nanomedicine and materdicine. *J. Mater. Chem. B* **2023**, *11* (24), 5350−5377.
(40) Suslick, K. S.; Hyeon, T.; Fang, M.; Cichowlas, A. A. Sonochemical Preparation of Nanostructured Catalysts. In *Advanced Catalysts and Nanostructured Materials*; Moser, W. R., Ed.; Academic Press: San Diego, 1996; Chapter 8, pp 197−212.
(41) Xu, H.; Zeiger, B. W.; Suslick, K. S. Sonochemical synthesis of nanomaterials. *Chem. Soc. Rev.* **2013**, *42* (7), 2555−2567.
(42) Hinman, J. J.; Suslick, K. S. Nanostructured Materials Synthesis Using Ultrasound. *Top. Curr. Chem.* **2017**, *375* (1), 12.
(43) Xu, Y.; Liu, J.; Liu, Z.; Chen, G.; Li, X.; Ren, H. Damaging Tumor Vessels with an Ultrasound-Triggered NO Release Nano-system to Enhance Drug Accumulation and T Cells Infiltration. *Int. J. Nanomed.* **2021**, *16*, 2597−2613.
(44) Gong, Z.; Dai, Z. Design and Challenges of Sonodynamic Therapy System for Cancer Theranostics: From Equipment to Sensitizers. *Adv. Sci.* **2021**, *8* (10), No. 2002178.
(45) Xing, X.; Zhao, S.; Xu, T.; Huang, L.; Zhang, Y.; Lan, M.; Lin, C.; Zheng, X.; Wang, P. Advances and perspectives in organic sonosensitizers for sonodynamic therapy. *Coord. Chem. Rev.* **2021**, *445*, No. 214087.
(46) Alghazwat, O.; Talebzadeh, S.; Oyer, J.; Copik, A.; Liao, Y. Ultrasound responsive carbon monoxide releasing micelle. *Ultrason. Sonochem.* **2021**, *72*, No. 105427.
(47) An, J.; Hu, Y.-G.; Li, C.; Hou, X.-L.; Cheng, K.; Zhang, B.; Zhang, R.-Y.; Li, D.-Y.; Liu, S.-J.; Liu, B.; Zhu, D.; Zhao, Y.-D. A pH/Ultrasound dual-response biomimetic nanoplatform for nitric oxide

https://doi.org/10.1021/acsabm.4c01165
ACS Appl. Bio Mater. 2024, 7, 7585−7594

gas-sonodynamic combined therapy and repeated ultrasound for relieving hypoxia. *Biomaterials* **2020**, *230*, No. 119636.
(48) Southam, H. M.; Smith, T. W.; Lyon, R. L.; Liao, C.; Trevitt, C. R.; Middlemiss, L. A.; Cox, F. L.; Chapman, J. A.; El-Khamisy, S. F.; Hippler, M.; Williamson, M. P.; Henderson, P. J. F.; Poole, R. K. A thiol-reactive Ru(II) ion, not CO release, underlies the potent antimicrobial and cytotoxic properties of CO-releasing molecule-3. *Redox Biol.* **2018**, *18*, 114−123.
(49) Opoku-Damoah, Y.; Zhang, R.; Ta, H. T.; Xu, Z. P. Simultaneous Light-Triggered Release of Nitric Oxide and Carbon Monoxide from a Lipid-Coated Upconversion Nanosystem Inhibits Colon Tumor Growth. *ACS Appl. Mater. Interfaces* **2023**, *15* (49), 56796−56806.
(50) Chen, W.; Goldys, E. M.; Deng, W. Light-induced liposomes for cancer therapeutics. *Prog. Lipid Res.* **2020**, *79*, No. 101052.
(51) Opoku-Damoah, Y.; Zhang, R.; Ta, H. T.; Jose, D. A.; Sakla, R.; Xu, Z. P. Lipid-encapsulated upconversion nanoparticle for near-infrared light-mediated carbon monoxide release for cancer gas therapy. *Eur. J. Pharm. Biopharm.* **2021**, *158*, 211−221, DOI: 10.1016/j.ejpb.2020.11.014.
(52) Zhang, W.; Zhang, J.; Zhang, H.; Cao, L.; Zhang, R.; Ye, Z.; Yuan, J. Development and application of a ruthenium(II) complex-based photoluminescent and electrochemiluminescent dual-signaling probe for nitric oxide. *Talanta* **2013**, *116*, 354−360.
(53) Dhara, K.; Lohar, S.; Patra, A.; Roy, P.; Saha, S. K.; Sadhukhan, G. C.; Chattopadhyay, P. A New Lysosome-Targetable Turn-On Fluorogenic Probe for Carbon Monoxide Imaging in Living Cells. *Anal. Chem.* **2018**, *90* (4), 2933−2938.
(54) Aouameur, D.; Cheng, H.; Opoku-Damoah, Y.; Sun, B.; Dong, Q.; Han, Y.; Zhou, J.; Ding, Y. Stimuli-responsive gel-micelles with flexible modulation of drug release for maximized antitumor efficacy. *Nano Res.* **2018**, *11* (8), 4245−4264.
(55) Andresen, E.; Resch-Genger, U.; Schäferling, M. Surface Modifications for Photon-Upconversion-Based Energy-Transfer Nanoprobes. *Langmuir* **2019**, *35* (15), 5093−5113.
(56) Duan, C.; Liang, L.; Li, L.; Zhang, R.; Xu, Z. P. Recent progress in upconversion luminescence nanomaterials for biomedical applications. *J. Mater. Chem. B* **2018**, *6* (2), 192−209.

https://doi.org/10.1021/acsabm.4c01165
ACS Appl. Bio Mater. 2024, 7, 7585−7594

Supporting Information

Ultrasound-Responsive Lipid Nanoplatform with Nitric Oxide and Carbon Monoxide Release for Cancer Sono-Gaso-Therapy

*Yaw Opoku-Damoah [1], Zhi Ping Xu[1,2 *], Hang T. Ta [1,3,4], and Run Zhang [1,*]*

[1] Australian Institute for Bioengineering and Nanotechnology, The University of Queensland, Brisbane, QLD 4072, Australia.

[2] Institute of Biomedical Health Technology and Engineering and Institute of Systems and Physical Biology, Shenzhen Bay Laboratory, Shenzhen 518107, PR China

[3] School of Environment and Science, Griffith University, Brisbane, QLD 4111, Australia

[4] Queensland Micro and Nanotechnology Centre, Griffith University, Brisbane, QLD 4111, Australia

Corresponding author:

Tel: +61 7 334 63806; E-mail: gordonxu@uq.edu.au; r.zhang@uq.edu.au.

Supplementary Figures

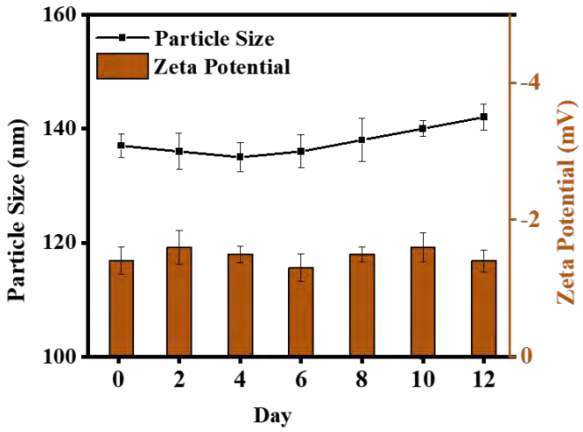

Figure S1. Colloidal stability of LUGCF in DMEM showing size and zeta potentials within 12 days.

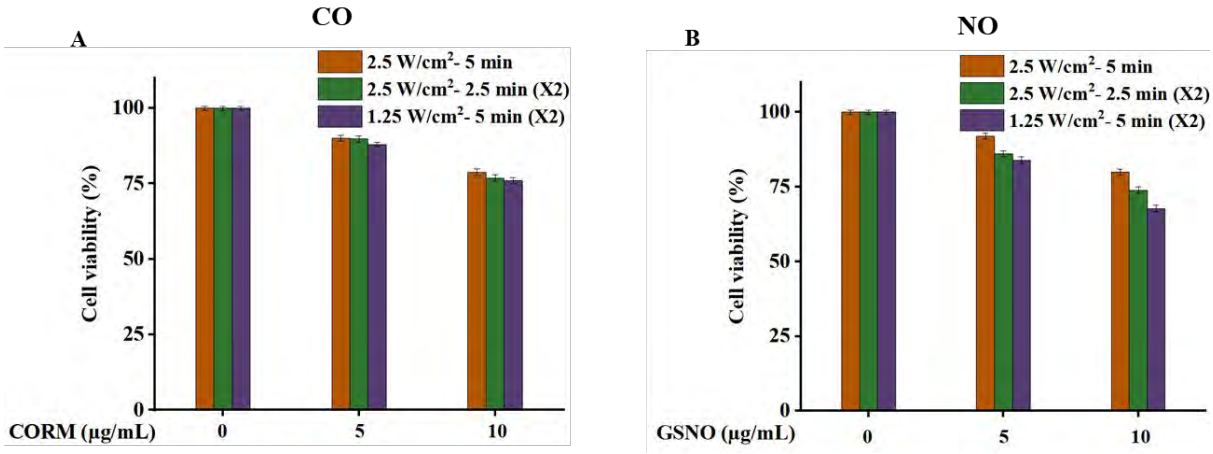

Figure S2. Cell viability assay optimization with fixed drug concentrations and different ultrasound conditions for **(A)** LUCF **(B)** LUGF.

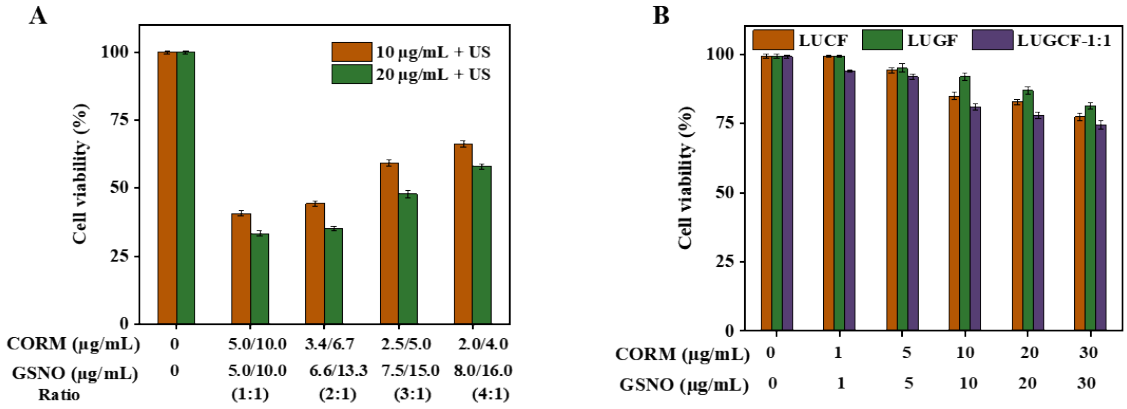

Figure S3. (A) MTT Assay for different ratios and combinations of LUGCF nanoformulation at 10 and 20 µg/mL after 48 h of incubation **(B)** 48 h MTT assay of LUCF, LUCF and LUGCF-1:1 nanoformulation without ultrasound application

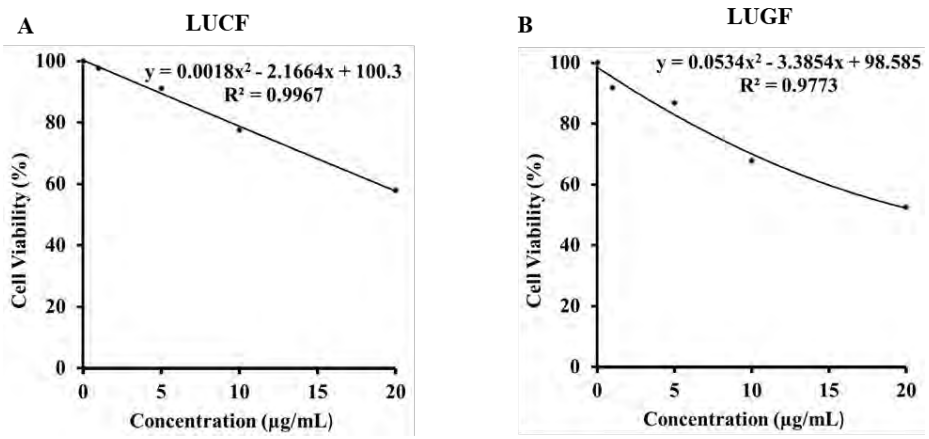

Figure S4. MTT Assay extrapolation for **(A)** LUCF and **(B)** LUGF at different concentrations showing cell viability profiles for known and calculated concentrations.

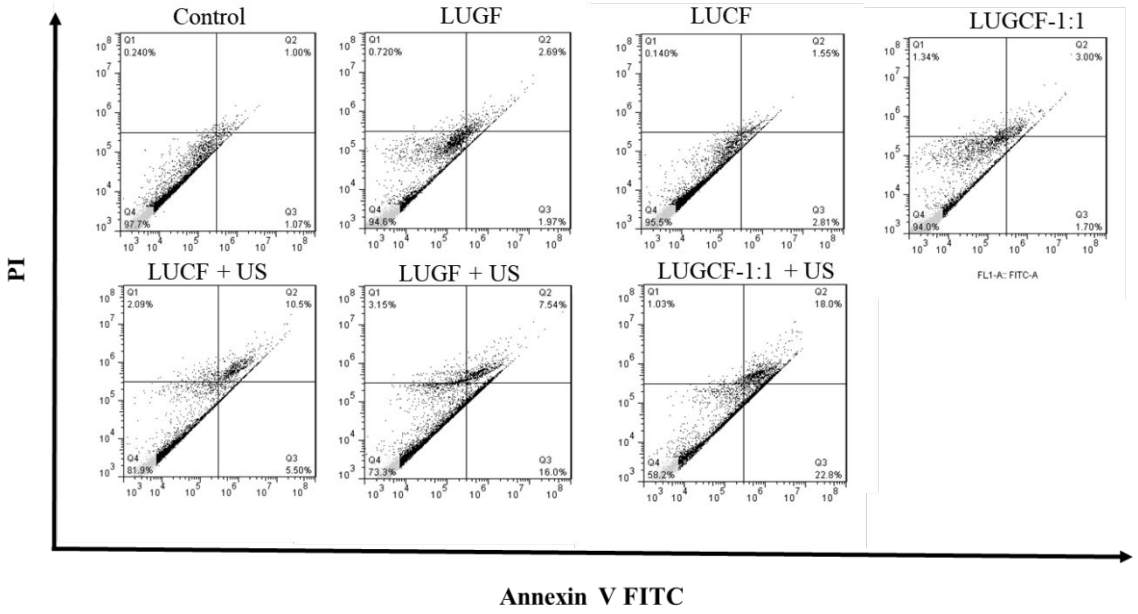

Figure S5. CT26 cell apoptosis assay for various nanoformulations after 24 h of total incubation. Ultrasound applied for 5 min at 4 h and another irradiation at 6 h (1.25 W/cm²).

Supplementary Tables

Table S1. MTT summary for combination therapy and corresponding LUGF/LUCF (with ultrasound treatment) with various ratios at a total of 10 and 20 µg/mL of the total [GSNO+CORM]. Cell viabilities extrapolated from tested groups after ultrasound application.

LUGF/LUCF (Ratio)	CORM/GSNO (Concentration)	LUCF Viability	LUGF Viability	LUGCF Viability	Combination index
1:1	5/5,	91.1	86.9	40.7	1.95
	10/10	77.7	67.8	33.3	1.60
2:1	3.4/6.7,	92.9	78.3	44.4	1.63
	6.6/13.3	86.1	63.0	35.1	1.54
3:1	2.5/7.5,	94.9	76.2	59.3	1.22
	5,15	89.5	59.8	47.8	1.11
4:1	2,8	96.0	74.9	66.2	0.95
	4,16	91.7	58.1	58.0	0.95

Table S2. IC_{50} values for various nanoformulations after 48 h of treatment.

Formulation	IC_{50} (µg/mL) CORM	IC_{50} (µg/mL) GSNO
LUCF	198.1	-
LUGF	-	211.3
LUCF + US	27.7	-
LUGF + US	-	22.4
LUGCF-1:1	117.5	117.5
LUGCF-1:1 + US	2.28	2.28

Table S3. Combination Indices for LUGCF nanoformulation with respect to single LUGF and LUCF nanoformulations

GSNO/CORM (Concentration)	LUCF Viability	LUGF Viability	LUGCF-1:1 Viability	Combination index
1/1	97.8	91.89	60.0	1.54
5/5	91.1	86.89	40.7	1.95
10/10	77.70	67.79	33.3	1.60
20/20	57.89	52.57	23.80	1.41
30/30	49.30	41.04	16.90	1.50

$$Combination\ Index\ (CI) = \frac{\text{Survival \% (LUGF)} \times \text{Survival \%(LUCF)}}{\text{Survival \% (LUGCF} - \text{1:1)}}$$

Average CI = $\sum$ CI/n

CI < 0.8 : asynergy; 0.8-1.2: additive; 1.2-1.4: mild synergy; 1.4-1.6: moderate synergy; >1.6: strong synergy [1-3]

Experimental Section

Materials

Cholesterol, 1,2-dioleoyl-sn-glycero-3-phosphocholine (DOPC), 1,2-dioleoyl-sn-glycero-3-phosphate (DOPA), 1,2-distearoyl-sn-glycero-3-phosphoethanolamine-N-(polyethylene glycol)-2000 (DSPE-PEG) and 1,2-dioleoyl-sn-glycero-3-phosphoethanolamine-N-(lissamine rhodamine B sulfonyl) (18:1 Liss Rhod PE), and 1,2-distearoyl-sn-glycero-3-phosphoethanolamine-N-[folate (polyethyleneglycol)-2000 (DSPE-PEG-FA) were purchased from Avanti Polar Lipids, USA. Lanthanides chloride hexahydrate ($TmCl_3 \cdot 6H_2O$, $NdCl_3 \cdot 6H_2O$, $YCl_3 \cdot 6H_2O$, $YbCl_3 \cdot 6H_2O$), ammonium fluoride (NH_4F), oleic acid (99% purity), sodium nitrite ($NaNO_2$), Nitrosyl tetrafluoroborate ($NOBF_4$), oleylamine (OM), and 1-octadecene (ODE) were obtained from Merck KgaA (Darmstadt, Germany). Dulbecco's Modified Eagle Medium (DMEM) and fetal bovine serum (FBS) were purchased from Gibco, USA. DCFH-DA ROS assay kit was purchased from Promokine. Annexin V-FITC cell apoptosis detection kit and JC-1 mitochondria assay kit were purchased from Invitrogen (by Thermofisher Scientific). All other chemicals used were obtained from Merck KgaA (Darmstadt, Germany) and were of HPLC or analytical grade.

Synthesis of Gas Releasing Molecules

$C_{30}H_{49}N_3Mn(CO)_3Br$ CORM was synthesized according to the method described previously by Sakla et al.[4] GSNO was also synthesized according to the method described by Hart et al. with a slight modification.[5] The NO molecule was prepared by adding 5mM of sodium nitrite ($NaNO_2$) to an equimolar amount (8.1 mmol) of glutathione (GSH) in 8 mL of deionized water containing HCl (2.5mL). The red mixture was stirred continuously for 40 min at 4 ºC before neutralization with acetone (10 mL) for 10 min. The final fine pale solid was centrifuged at

2000 x g for 3 min and washed with excess ice-cold water, acetone and ether to produce a pale red solid which was kept in a desiccator to dry.

Cell Culture

Murine colorectal carcinoma cells (CT26) were grown in 90% DMEM supplemented with 10% FBS 100 U/mL penicillin, and 100 mg/mL streptomycin. Exponentially growing cultures were maintained in a humidified chamber containing 5% CO_2 at 37 ℃ throughout the cell studies.

References

1. Ito, A.; Fujioka, M.; Yoshida, T.; Wakamatsu, K.; Ito, S.; Yamashita, T.; Jimbow, K.; Honda, H., 4-S-Cysteaminylphenol-loaded magnetite cationic liposomes for combination therapy of hyperthermia with chemotherapy against malignant melanoma. *Cancer Science*, **2007,** *98* (3), 424-430.

2. Liu, J.; Sun, L.; Li, L.; Zhang, R.; Xu, Z. P., Synergistic Cancer Photochemotherapy via Layered Double Hydroxide-Based Trimodal Nanomedicine at Very Low Therapeutic Doses. *ACS Applied Materials & Interfaces* **2021,** *13* (6), 7115-7126.

3. Li, B.; Tang, J.; Chen, W.; Hao, G.; Kurniawan, N.; Gu, Z.; Xu, Z. P., Novel theranostic nanoplatform for complete mice tumor elimination via MR imaging-guided acid-enhanced photothermo-/chemo-therapy. *Biomaterials* **2018,** *177*, 40-51.

4. Sakla, R.; Jose, D. A., Vesicles Functionalized with a CO-Releasing Molecule for Light-Induced CO Delivery. *ACS Appl Mater Interfaces* **2018,** *10* (16), 14214-14220.

5. Hart, T. W., Some observations concerning the S-nitroso and S-phenylsulphonyl derivatives of L-cysteine and glutathione. *Tetrahedron Letters* **1985,** *26* (16), 2013-2016.